Taper Design and Wood Selection for Reverse Engineering of Bows for String Instruments

FRANCIS J. TESTA

34 Chipping Ridge, Fairport, NY 14450
ftesta@rochester.rr.com

Abstract

After discussing the difficult conflict between stiffness and density in producing professional-quality bows, we derive the new taper required to produce the same local stiffness as the target bow from a blank of possibly different modulus of elasticity. Furthermore, we prove that by selecting wood with the same value of the parameter $\mu = \frac{E}{\rho^2}$ *as the target bow, both the mechanical bending and mass properties between the head and forward frog position of the target can be reproduced exactly. This parameter then serves as a general basis for wood selection, replacing the speed of sound measurement, shown to penalize the value of lower density wood while inflating that of higher density. In outlining a procedure for reverse engineering, modeling of the target bow, geometry and methods for estimating the modulus and density of bow or blank are presented together with a derivation of the associated camber and its relationship to maximum hair tension and proximity to full camber. The Tourte taper is discussed with particular emphasis on its close approximation to linear stiffness as a function of position along the stick. Using a linearized stiffness model of a particular bow by Dominique Peccatte, tapers are presented for two blanks with the same value of* μ*, having significantly different modulus and density, but with each reproducing the same local stiffness and mass properties between the head and frog. Stiffness plots of four bows that reproduce the same linearized local stiffness are shown together with that of the Peccatte. Data on modulus, density, and damping ratio from a sample of 50 violin bow blanks is also presented, demonstrating the implicit problem with wood selection based on speed of sound.*

1. INTRODUCTION

The fundamental problem in producing professional-quality bows for string instruments lies in coping with the conflict between wood stiffness and density. Although high wood stiffness helps in achieving the desired mechanical bending properties of the bow, higher density only adds weight, making it more difficult to satisfy the typical desired weight and moment properties in a finished bow. While the contribution to the weight of a cross section is uniform, the resulting stiffness is proportional to the cross-sectional moment of inertia, dependent on the square of the distance of the mass from the bending axis. The wood toward the surface of the cross section contributes more to the stiffness than the wood toward the center. Therefore, while any wood could be used to achieve the necessary stiffness by leaving it thicker, most would greatly exceed the typical weight constraints. Historically, this has led to Pernambuco as the wood of choice for modern bows. It is well-known [1,2] that Pernambuco of higher modulus typically has higher density and this property has caused blanks of higher modulus and density to be viewed as always more desirable, and regarded "floaters," specific gravity less than one, as wood not capable of producing high-quality bows. Furthermore, because of the delicate balance between mass and stiffness in bow design, a current belief [3] among bowmakers is that it is only possible to either build in the needed stiffness by taper design or achieve the desired mass properties, but not both.

In what follows, we prove that both the desired stiffness and mass properties of the bending section of the bow can be reproduced exactly

through wood selection based on the parameter $\mu = \frac{E}{\rho^2}$, where E is the modulus of elasticity and ρ is the specific gravity, providing identical units for both E and μ. This results in wood with the same value of μ being completely equivalent in producing a bow with the same bending, mass, and moment properties between the head and frog and serves as the basis for reverse engineering a desired finished bow. Furthermore, this elevates the value of some floaters to the equal of their more dense alternatives. Although estimates for wood properties are usually based on the simplifying assumption that they are constants, clearly they are very likely to change as wood is removed in producing a finished bow. Therefore, the procedure presented here is an iterative one, repeatedly estimating the properties of the wood that remains as some wood is removed and modifying the target taper accordingly.

2. GENERAL DESCRIPTION

This analysis for reverse engineering of bows for string instruments is based on the realization that, for given frog and head heights, the mechanical bending properties of a bow are completely determined by the modulus of elasticity and cross-sectional moment of inertia as functions of position along the stick, together with the initial camber at zero tension in the hair. This requires solving the problem of designing the taper in a given piece of wood that will reproduce the same local stiffness as the desired target bow as a function of position along the stick. Given the complexity of any alternative, we have made the simplifying assumption that both the modulus of elasticity and density are constants. The geometry of the target bow is obtained using a model of the cross-sectional shape from graduation measurements, producing representations of the cross-sectional area and moments of inertia as a function of arc length along the stick. In a simple cantilever static deflection experiment with the bow clamped at the forward frog position and a small vertical load just behind the head, the measured deflection then determines the average modulus of elasticity necessary to produce that deflection given the modeled geometry of the bow.

The mass of the stick together with the location of the center of mass gives two equations solved for the density and estimate of the volume of the head. In a finished bow, this approach also requires estimating the mass and center of mass of the wrapping above the frog, together with the model of the frog section.

The conventional wisdom among bowmakers has been that tightening the hair in a bow should simply have the effect of gradually undoing the camber, eventually resulting in the stick reaching a straight line at maximum tension in the hair. While this level of tension is usually never used in actual playing, this design concept seems reasonable and has been incorporated here. This assumption together with an analysis of the tapered curved beam boundary value problem then establishes a unique relationship between the taper and camber, where the appropriate camber defined by the maximum desired tension in the hair, is computed directly from the designed taper and modulus of elasticity, while respecting the maximum camber constraint for the effective frog and head heights.

Although designing the taper in a blank that reproduces the desired local stiffness in a target bow is necessary in any reverse engineering strategy, coping with likely different mass distribution from a new taper in a blank with different density complicates the problem. In what follows, a wood selection parameter, computed from the modulus of elasticity and specific gravity, completely solves this problem, reproducing the weight and important moment properties of the bending section of the bow. Furthermore, this parameter provides the basis for wood selection leading to the most successful outcome.

3. TAPER

Measuring the arc length s of the stick from a point just behind the head, the stiffness or flexural rigidity at a given value of s is the product of the modulus of elasticity and the cross-sectional moment of inertia. In designing the taper for a blank of modulus E_b to realize the same local bending properties as a desired target bow with modulus E_t, the local stiffness of the target as a function of s must be reproduced. While knowledge of the taper in the target bow is necessary,

it is in general, not the taper to be used in the new design. For example, for a circular cross section of diameter D and modulus E, the stiffness is given by

$$EI = \frac{\pi E D^4}{64} \tag{1}$$

If the target bow has modulus E_t and the blank has modulus E_b, the diameter of the target taper must be multiplied by the same factor at every point to realize the local stiffness of the target from the wood in the blank with a different modulus. For the new taper defined by

$$D_b = \left(\frac{E_t}{E_b}\right)^{\frac{1}{4}} D_t, \tag{2}$$

its stiffness is then given by

$$E_b I_b = \frac{\pi E_b D_b^4}{64} = \frac{\pi E_t D_t^4}{64} = E_t I_t \tag{3}$$

The important conclusion drawn from this is that a difference in modulus between blank and target requires a different taper in the blank and not simply the same taper with different overall thickness, to achieve the same local stiffness as the target bow. This approach provides knowledge of the starting taper to be used in roughing out a particular blank and offers a workable successful outcome for blanks of lower modulus and density. For example, in the case where $E_b < E_t$, the multiplying factor is greater than one and will cause more wood to be added to the target diameter as its diameter increases. Such a blank might be made useless by starting with a taper more suitable in a stronger blank.

The mass properties of the bow are determined by the cross-sectional area, $A(s)$ as a function of arc length along the stick measured from just behind the head and computed from the taper, with its corresponding mass per unit length $\rho A(s)$. The weight of the stick between the head and the forward frog position and its important moments with respect to that position are then given by

$$w' = \rho \int_0^{L_s} A(s) ds \tag{4}$$

$$m' = \rho \int_0^{L_s} x_m(s) A(s) ds \tag{5}$$

$$i' = \rho \int_0^{L_s} x_m(s)^2 A(s) ds \tag{6}$$

where, L_s is the arc length of the stick between the head and the forward frog position and $x_m(s)$ is the horizontal moment arm for the cross section at s with respect to the forward frog position. The horizontal location of the center of mass of the bending section of the bow from the forward frog position then follows from Eqns. (4) and (5).

$$cm = \frac{m'}{w'}. \tag{7}$$

While the stiffness in Eqn. (1) is proportional to D^4, the mass and the moments with respect to the forward frog position are only proportional to D^2, accounting for the mysterious conflict between stiffness and density.

4. WOOD SELECTION

Given the desired playing properties in a professional-quality bow, the conflict between stiffness and density, places difficult demands on wood selection. While the contribution to weight of a cross section is uniform, the stiffness is proportional to the cross-sectional moment of inertia, dependent on the square of the distance of the mass from the bending axis. The wood toward the surface of the cross section contributes more to the stiffness than the wood toward the center. Therefore, while any wood could be used to achieve the necessary stiffness by leaving it thicker, most would greatly exceed the typical weight constraints, historically leading to Pernambuco as the wood of choice for modern bows.

As shown in Eqn. (3), the local stiffness of a target bow with taper D_t can be reproduced from a blank of a different modulus of elasticity E_b from the taper obtained by multiplying the target taper by the constant, $\left(\frac{E_t}{E_b}\right)^{\frac{1}{4}}$. While this is a necessary condition in reverse engineering a target bow, the weight, moment, and moments of inertia of the resulting bow must deal with the corresponding difference in densities between blank and target. For Pernambuco of modulus

of elasticity E and density ρ, we define the parameter μ given by

$$\mu = \frac{\mathrm{E}}{\rho^2} \tag{8}$$

Viewing density in its equivalent dimensionless form of specific gravity, μ can conveniently be represented with the same units as the modulus of elasticity. For a target bow and blank with the same value of μ, this results in the condition

$$\frac{E_\mathrm{t}}{E_\mathrm{b}} = \left(\frac{\rho_\mathrm{t}}{\rho_\mathrm{b}}\right)^2 \tag{9}$$

Using the blank taper D_b in Eqn. (2) that produces the same local stiffness as the target, the cross-sectional area is transformed by the square of the same factor.

$$A_\mathrm{b} = \left(\frac{E_\mathrm{t}}{E_\mathrm{b}}\right)^{\frac{1}{2}} A_\mathrm{t} = \left(\frac{\rho_\mathrm{t}}{\rho_\mathrm{b}}\right) A_\mathrm{t} \tag{10}$$

From this, it follows that the mass per unit length, together with both the weight and moments of the blank taper between the head and forward frog position, are identical to those of the target.

$$\rho_\mathrm{b} A_\mathrm{b} = \rho_\mathrm{t} A_\mathrm{t} \tag{11}$$

$$w'_\mathrm{b} = \rho_\mathrm{b} \int_0^{L_\mathrm{s}} A_\mathrm{b}(s) ds = \rho_\mathrm{t} \int_0^{L_\mathrm{s}} A_\mathrm{t}(s)\, ds = w'_\mathrm{t} \tag{12}$$

$$\begin{aligned} m'_\mathrm{b} &= \rho_\mathrm{b} \int_0^{L_\mathrm{s}} x_\mathrm{m}(s) A_\mathrm{b}(s) ds \\ &= \rho_\mathrm{t} \int_0^{L_\mathrm{s}} x_\mathrm{m}(s) A_\mathrm{t}(s) ds = m'_\mathrm{t} \end{aligned} \tag{13}$$

$$\begin{aligned} i'_\mathrm{b} &= \rho_\mathrm{b} \int_0^{L_\mathrm{s}} x_\mathrm{m}(s)^2 A_\mathrm{b}(s) ds \\ &= \rho_\mathrm{t} \int_0^{L_\mathrm{s}} x_\mathrm{m}(s)^2 A_\mathrm{t}(s) ds = i'_\mathrm{t} \end{aligned} \tag{14}$$

We now have the remarkable result that when a blank is selected with the same value of μ as the target bow, both the local stiffness and all mass properties of the target between the head and forward frog position are reproduced exactly using the computed taper D_b in Eqn. (2). This demonstrates that blanks with the same value of μ are completely mechanically equivalent in terms of their possible stiffness and weight properties between the head and frog in a finished bow. The differences in cantilever mode frequencies between the blank taper and target taper are then completely determined by the differences in the heads of the two bows. The fundamental mode frequency can then be tuned by adjusting the head shape without modifying the important effective head height, to compensate for the possible different density of the blank. For a blank with lower density than the target, a small mass could simply be added without the need to change the head shape. The total weight and balance properties of the finished bow are then managed by grip, frog, and button selection.

From a sample of 50 violin bow blanks, the process described in Sections 5 and 6 was used to determine estimates for their modulus and density and plotted in Fig. 1 together with a linear least squares fit, demonstrating the expected increasing trend in their relationship. The color of the points map their corresponding values of μ to a light-to-dark color map, with light the smallest and dark the largest values. With points of similar shades having similar values of μ, clearly some lower density and modulus blanks are really competitive with their typically more prized higher density alternatives.

Given the interest in the speed of sound as a basis for wood selection, its relationship to the modulus and density [2,4] is given by

$$c = \sqrt{\frac{E}{\rho}} \tag{15}$$

Since the square root function is monotonic, this is equivalent to screening the wood on the basis of c^2, easily expressed in terms of the wood selection parameter μ and density ρ given by

$$c^2 = \rho\ \mu \tag{16}$$

Having shown that μ is the definitive measure of the mass and stiffness outcome between the head and the frog, wood selection based solely on the speed of sound, inflates the value of high-density wood, $\rho > 1$, while penalizing wood of low density and leads to the false perception that all "floaters" are worthless. Computing c from Eqn. (15), this misconception is

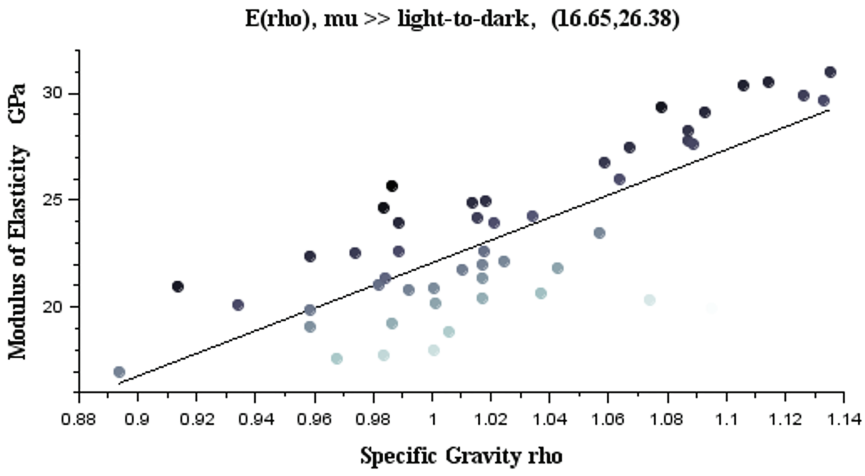

Figure 1. Variation of modulus with specific gravity and including light-to-dark point shade mapped to increasing values of the parameter μ on the interval (16.65, 26.38).

illustrated in Fig. 2 by the following analogous plot with the increasing values of the speed of sound mapped light-to-dark, clearly reducing interest in lower modulus and lower density wood given higher concentration of darker points among higher density blanks.

This implicit bias of wood selection based on velocity of sound is further demonstrated by the following scatter plots in Figs. 3 and 4 of $\mu(\rho)$ and $c(\rho)$ and their respective linear least squares trend lines. The range of values of μ is on the interval [16.6, 26.4], with the range of c on [4237, 5239]. The colors of the points have been preserved and the vertical sizes of the plots were adjusted to represent each vertical range with same length on the page.

The significantly steeper slope of the linear trend line in $c(\rho)$ demonstrates the implicit

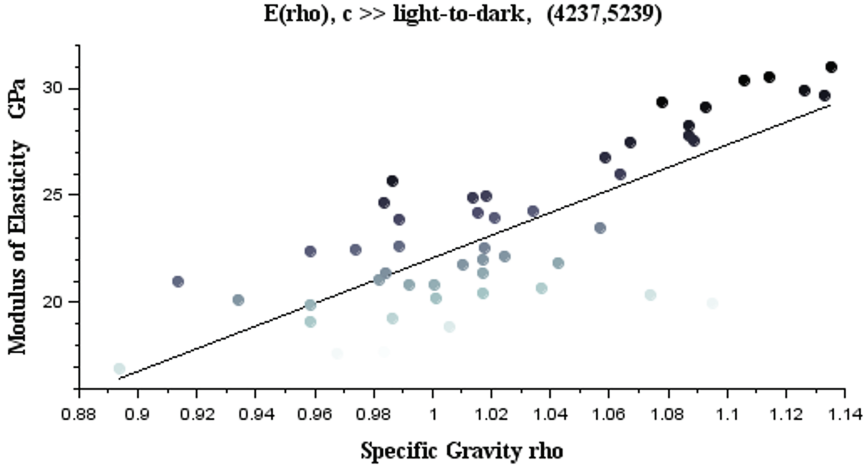

Figure 2. Variation of modulus with specific gravity and including light to dark point shade mapped to increasing values of the speed of sound, c on the interval (4237, 5239) in m/s.

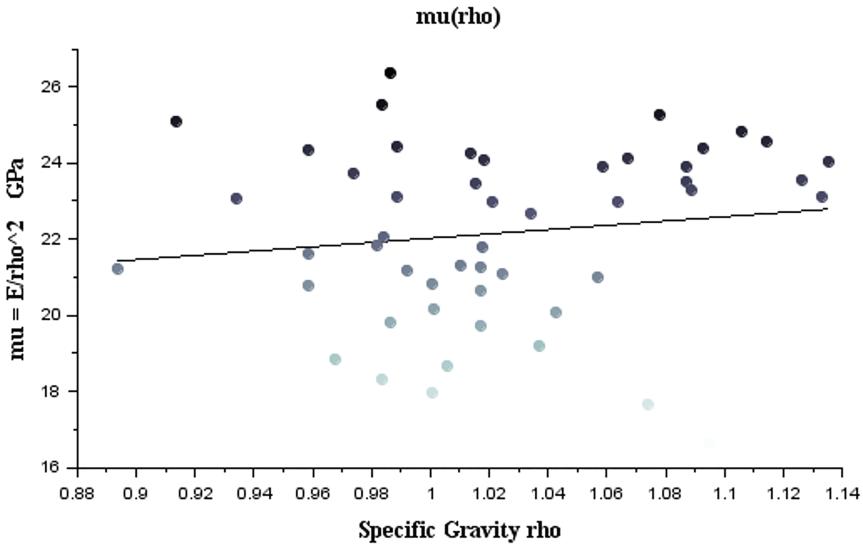

Figure 3. Plot of $\mu(\rho)$ together with its least squares linear trend line.

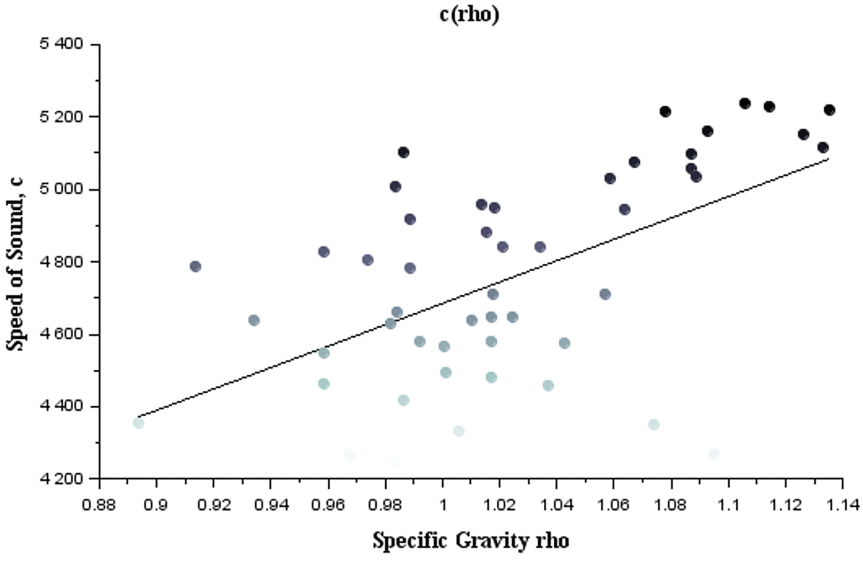

Figure 4. Plot of $c(\rho)$ together with its least squares linear trend line.

penalty against lower density wood based on speed of sound measurements when compared with the more accurate wood selection parameter μ.

Since the chances of making a high-quality bow are improved by either increasing the modulus or decreasing the density, it is obvious that blanks with the largest values of $\mu = \frac{E}{\rho^2}$ are the most desirable for the possible mechanical outcome and should generally be the basis of wood selection. As shown in Section 5, it is

noteworthy [5] that the wood at the corners of an octagonal cross section given their greater distance from the neutral axis, offers an edge to the possible outcome for octagonal bows given the same piece of wood.

5. CROSS-SECTIONAL SHAPE

The local stiffness of a beam at any point is proportional to the cross-sectional moment of inertia, or second moment of the area about a bending axis. While for a straight beam the neutral axis is typically through the centroid of the cross section, this is not the case for curved beams [6] and it is dependent on the local curvature. Since the actual curvature in a bow is relatively small, it is likely that the cross section centroid is close to the neutral axis. Therefore, the effective head and frog heights can be approximated by distance of the line of action of the hair from the centroid of the cross section.

Moments of inertia and area of the simple shapes of a circle and rectangle in Figs. 5 and 6 are easily found as given by

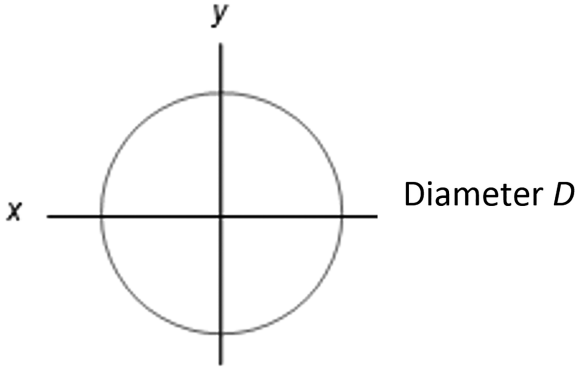

Figure 5. Round cross section.

$$I_x = I_y = \frac{\pi D^4}{64}, \quad A = \frac{\pi D^2}{4} \tag{17}$$

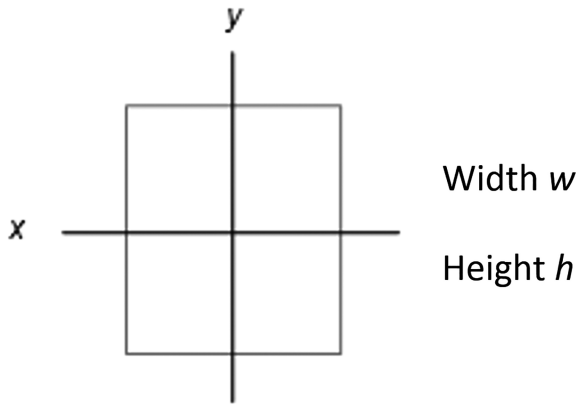

Figure 6. Rectangular cross section.

$$I_x = \frac{w\,h^3}{12}, \quad I_y = \frac{h\,w^3}{12}, \quad A = wh \tag{18}$$

While the rectangular shape is useful in modeling a typical bow blank, the case of either an "octagonal" or "round" bow is more complicated. Furthermore, these descriptions are only qualitative and, therefore, a geometric model of the bow must account for the actual possibly somewhat "oval" nature of the cross-sectional shapes. To that end, the case of a symmetric octagon in Fig. 7 can be represented using four different thicknesses around the stick, *V*, *U*, *H*, and *L*. Straightforward but somewhat tedious integration yields the moments of inertia and cross-sectional area given by

$$I_x = \frac{V^3\left(\sqrt{2}\,U + \sqrt{2}\,L\right)}{24} - \frac{V^4}{16} - \frac{\left(\sqrt{2}\,U - H\right)^4}{96} - \frac{\left(\sqrt{2}\,L - H\right)^4}{96} \tag{19}$$

$$I_y = \frac{H^3\left(\sqrt{2}\,U + \sqrt{2}\,L\right)}{24} - \frac{H^4}{16} - \frac{\left(\sqrt{2}\,U - V\right)^4}{96} - \frac{\left(\sqrt{2}L - V\right)^4}{96} \tag{20}$$

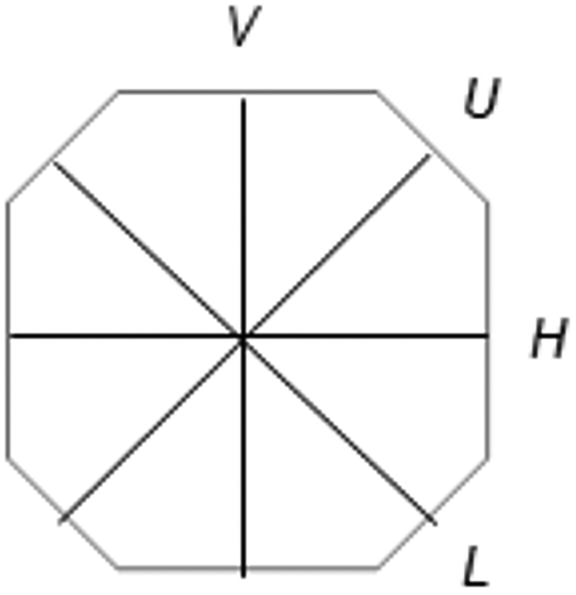

Figure 7. Octagonal cross section.

$$A = \frac{V\left(\sqrt{2}\ U + \sqrt{2}\ L\right)}{2} - \frac{V^2}{2} - \frac{\left(\sqrt{2}\ U - H\right)^2}{4} - \frac{\left(\sqrt{2}\ L - H\right)^2}{4} \tag{21}$$

For a regular octagon of thickness D, these reduce to

$$I_x = I_y = \frac{D^4\left(32\sqrt{2} - 40\right)}{96} \tag{22}$$

$$A = 2D^2\left(\sqrt{2} - 1\right) \tag{23}$$

It is noteworthy that comparison of the regular octagon and round cross sections shows that, while the octagonal area increases by a factor of 1.055, the cross-sectional moment of inertia is increased by a factor of 1.115, accounting for the advantage of the octagonal cross section in dealing with blanks of lesser quality.

For the "round" case in Fig. 8, rather than use an ellipse or some other constrained shape to represent the somewhat oval cross section in real bows, we again measure the thickness at four equidistant angles around the stick, *V*, *U*, *H*, and *L*.

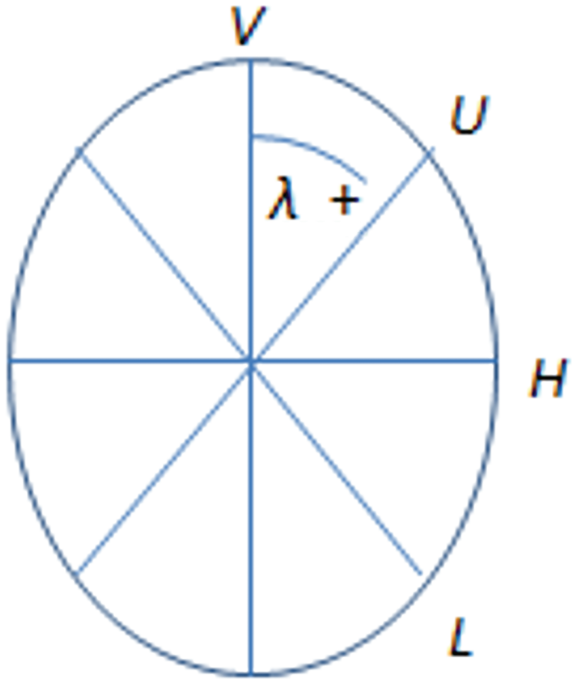

Figure 8. Oval cross section.

Assuming symmetry, a periodic cubic spline is then fitted to this graduation data to obtain a representation of the stick diameter, $D(\lambda)$, as a function of the angle λ, measured clockwise positive from a vertical line through the centroid and looking toward the head. Direct integration in polar coordinates then gives the vertical and horizontal moments of inertia, I_x and I_y, together with the cross-sectional area A.

$$I_x = \int_0^{\pi} \frac{D^4(\lambda)}{32} cos^2(\lambda) d\lambda, \qquad I_y = \int_0^{\pi} \frac{D^4(\lambda)}{32} sin^2(\lambda) d\lambda \tag{24}$$

$$A = \int_0^{\pi} \frac{D^2(\lambda)}{4} d\lambda \tag{25}$$

6. MODULUS OF ELASTICITY

For either a bow blank, partly finished or actual finished bow, the average modulus of elasticity in the vertical plane is obtained by a simple

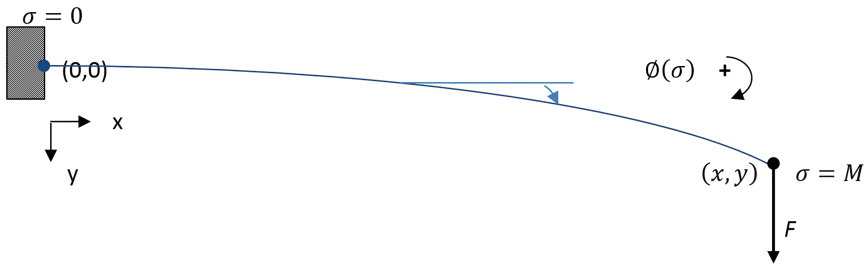

Figure 9. Cantilever at forward frog position.

cantilever static deflection experiment [7] with the stick clamped at the frog end, and the arc length σ, measured from the clamped position as shown in Fig. 9.

From this formulation in terms of the tangent angle $\varnothing$ with initial camber $\varnothing_0$ as functions of arc length σ, the strain energy U for this elastic and conservative system [6,8,9] is given by

$$U = \int_0^M \frac{EI}{2} (\varnothing' - \varnothing_0')^2 \, d\sigma \tag{26}$$

Since the vertical Cartesian coordinates for the final and initial positions of the end at the point load are in the form

$$y = \int_0^M \sin\varnothing d\sigma \quad y_0 = \int_0^M \sin\varnothing_0 d\sigma, \tag{27}$$

the deflection δ under the point load F is then found as $\delta = y - y_0$. The potential energy Ω of the external load is then given by

$$\Omega = -F(y - y_0) \tag{28}$$

Employing the principle of stationary potential energy on total potential energy $\Pi = U + \Omega$

$$\delta \Pi = 0 \tag{29}$$

yields the nonlinear boundary value problem

$$\left[EI\left(\varnothing' - \varnothing_0'\right)\right]' + F\cos\varnothing = 0 \tag{30}$$

$$\varnothing(0) = 0, \quad \left[EI\left(\varnothing' - \varnothing_0'\right)\right]_{\sigma=M} = 0 \tag{31}$$

with the constant modulus E, and the cross-sectional moment of inertia $I(\sigma)$ under the action of the point load F.

Modeling the cross-sectional shape using methods specific to rectangles, octagons, or curves as appropriate, graduation measurements at 20-mm intervals along the stick are then used to compute a spline model of the moment of inertia $I(\sigma)$ as a function of σ. The initial camber $\varnothing_0$ is simply zero for a straight bow blank or roughed out bow, or assumed to be the camber that is undone by tightening the hair in a finished bow. While this may not be precisely true in every case, the errors in this assumption are likely to be small.

With the bow clamped at the forward frog position and a small magnet on the head of the bow behind the mortise, a linear Hall-effect transducer mounted vertically on an x–y microscope stage and dial indicator resting on the stage, are used to measure the deflection of the stick under the applied load F. An estimate for the average Young's modulus E in the vertical plane is then obtained by embedding the above boundary value problem inside a root finding algorithm, thereby computing the value of E that gives the measured deflection given the geometry modeled from the measured graduation data. This was computed using a Picard [10] iteration algorithm in Scilab and this process applied to a target bow provides an estimate for its average modulus E_t.

The mass of the stick together with the location of the center of mass gives two equations, solved for the density and estimate of the volume of the head. In a finished bow, this approach requires estimating the mass and center of mass of the wrapping above the frog, together with the model of the frog section. Alternatively, measurement of the speed of sound could also be used to estimate the density ρ from the modulus E but measurement error is approximately doubled because of the square of the speed.

7. MODEL OF TARGET BOW

Although bows are either round or octagonal, historically, sometimes the cross section is made taller than it is wide producing more stiffness in the vertical plane to compensate for a weaker piece of wood but likely at the expense of lateral stiffness. Therefore, an actual round model equivalent to the target bow vertical plane stiffness is a better choice as the basis for the taper design.

With arc length s along the stick measured from just behind the head, these area moments of inertia are computed at 20-mm intervals and spline models produce the functions of arc length, $I_x(s)$ and $I_y(s)$. Using only the vertical plane area moment of inertia for a round cross section in Eqn. (17), we obtain an equivalent actual round model of the target bow taper given by

$$D_R(\sigma) = \left(\frac{64\ I_x(s)}{\pi}\right)^{\frac{1}{4}} \tag{32}$$

An analogous equivalent regular octagonal model can also be computed from Eqn. (22) if preferred, especially in the case of blanks of smaller values of μ.

$$D_O(\sigma) = \left(\frac{96\ I_x(s)}{32\sqrt{2}-40}\right)^{\frac{1}{4}} \tag{33}$$

Since the stick is octagonal in the frog section, modeling a round bow requires a small transition region, typically under the winding, between the round and octagonal cross-sectional area and moment of inertia.

8. CAMBER

The conventional wisdom among bowmakers is that the ideal camber is that which is simply undone by tightening the hair, resulting in a straight line for the bow. The static bending problem under tensioning of the hair shown in Fig. 10 can be analyzed using an analogous formulation with arc length parameter s, tangent angle $\theta(s)$, initial camber $\theta_0(s)$, bow arc length L_T to the frog under hair tension T, and effective head and frog heights a and b, respectively. It is important to note that a and b are distances of the hair tension from the neutral axis of the bow and not the actual heights of the head and frog. Since the frog moves back from its forward position in this analysis, the origin of arc length is now chosen at a point behind the head.

The strain energy U for this elastic and conservative system [6,8,9] is given by

$$U = \int_0^{L_T} \frac{EI}{2}(\theta' - \theta_0')^2 ds, \tag{34}$$

with the potential energy Ω of the external load in the form

$$\Omega = -T(l_0 - l) \tag{35}$$

where,

$$l = b\ sin\ \theta(L_T) - a\sin\theta(0) + \int_0^{L_T} \cos\theta(s) ds \tag{36}$$

The total potential energy is then $\Pi = U + \Omega$, and employing the principle of stationary potential energy,

$$\delta\ \Pi = 0 \tag{37}$$

yields the nonlinear boundary value problem

$$\left[EI\left(\theta' - \theta_0'\right)\right]' + T\sin\theta = 0 \tag{38}$$

$$\left[EI\left(\theta' - \theta_0'\right)\right]_{s=0} + Ta\cos\theta(0) = 0 \tag{39}$$

$$\left[EI\left(\theta' - \theta_0'\right)\right]_{s=L_f} + Tb\cos\theta(L_T) = 0 \tag{40}$$

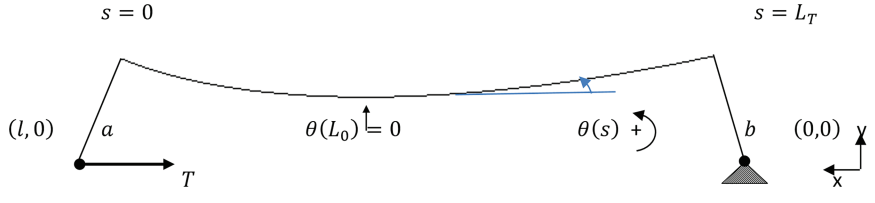

Figure 10. Static bending under hair tension.

While this is a difficult nonlinear problem, it can be used to reveal the intimate and unique relationship between the taper and the camber provided by the conventional wisdom assumption. This straight line assumption means that there must exist a maximum tension $\overline{T}$ and a frog location L_S such that the solution to the abovementioned problem is $\theta(s) = \beta$ a constant. From Eqn. (38), it follows that

$$\left[EI\theta_0'\right]' = \overline{T}\sin\beta \tag{41}$$

Direct integration with respect to s gives

$$EI\theta_0' = \overline{T}\mathrm{s}\sin\beta + c \tag{42}$$

where, $c = \overline{T}a\cos\beta$ and $\tan\beta = \dfrac{b-a}{L_S}$ follow from the boundary conditions. Solving for the curvature θ_0', we then have

$$\theta_0'(s) = \frac{\overline{T}(\mathrm{s}\sin\beta + a\cos\beta)}{EI(s)} \tag{43}$$

It is noteworthy that in the trivial special case of constant cross-sectional moment of inertia I and identical head and frog heights, $\beta = 0$ and the curvature $\theta_0'(s)$ is a constant as expected.

$$\theta_0'(s) = \frac{\overline{T}a}{EI} \tag{44}$$

A quadrature expression for the camber is then given by

$$\theta_0(s) = g(s) + \theta_0(0) \tag{45}$$

where,

$$g(s) \equiv \int_0^s \frac{\overline{T}(\mathrm{s}\sin\beta + a\cos\beta)}{EI(s)}ds \tag{46}$$

Furthermore, with the definitions

$$u(s) \equiv \int_0^s \sin g(s)ds \quad v(s) \equiv \int_0^s \cos g(s)ds, \tag{47}$$

it can be shown that

$$\theta_0(0) = \tan^{-1}\left\{\frac{b\cos g(L_T) - u(L_T) - a}{v(L_T) + b\sin g(L_T)}\right\} \tag{48}$$

The Cartesian coordinates for the camber of the neutral axis are then found in the form

$$\begin{aligned} x_0(s) &= \int_0^s \cos\theta_0(s)ds \\ &= v(s)\cos\theta_0(0) - u(s)\sin\theta_0(0) \end{aligned} \tag{49}$$

$$\begin{aligned} y_0(s) &= \int_0^s \sin\theta_0(s)ds + a\cos\theta_0(0) \\ &= u(s)\cos\theta_0(0) + v(s)\sin\theta_0(0) \\ &\quad + a\cos\theta_0(0) \end{aligned} \tag{50}$$

The maximum tension, $\overline{T}$, when the bow is straight, is controlled by the amount of camber, with full camber defined by the bottom of the stick touching the table for the given frog and head heights at the point $s = L_0$. It is easily shown that the two unknowns $\overline{T}$ and L_0 can be obtained from the two constraint equations

$$\theta_0(L_0) = g(L_0) + \theta_0(0) = 0 \tag{51}$$

$$\begin{aligned} y_0(L_0) &= u(L_0)\cos\theta_0(0) + v(L_0)\sin\theta_0(0) \\ &\quad + a\cos\theta_0(0) = \frac{V(L_0)}{2} + \varepsilon \end{aligned} \tag{52}$$

where, $V(L_0)$ is the vertical thickness of the stick at L_0 and ε is the distance between the bottom of the stick and the table.

9. TOURTE TAPER

It is well-known that the taper in Tourte bows, as modeled by Vuillaume [11], has the interesting property that the stiffness as a function of position in the bow closely approximates a linear function [12]. While not yet understood, this really has some intuitive appeal and is supported by several bows for which I was able to measure both the graduations and estimate the modulus in the cantilever experiment. Although my analysis now uses four measurements around the stick to model the cross-sectional shape, the plots shown in Figs. 11 and 12 are from an earlier effort when only horizontal and vertical graduation data were taken, using an ellipse to model the cross-sectional shape. Both the vertical and horizontal stiffness are shown, with the linear stiffness over much of the stick clearly evident, particularly in the Peccatte. The more oval cross-sectional shape in the Tourte contributed to its somewhat excessive lateral flexibility.

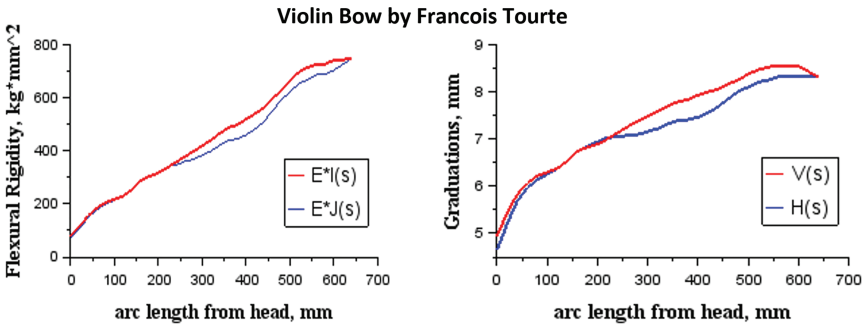

Figure 11. Local stiffness and graduations as functions of arc length for bow by Tourte.

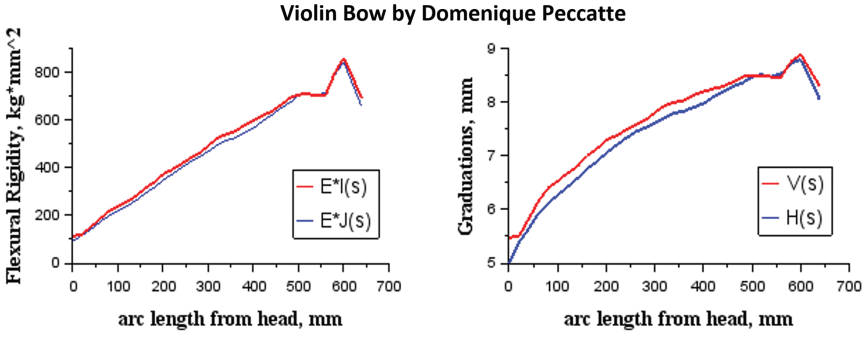

Figure 12. Local stiffness and graduations as functions of arc length for bow by Peccatte.

While utilizing such an oval design gains more vertical strength, lateral problems can be minimized by using a round cross section derived from the vertical stiffness as described in Section 7.

Estimates for the modulus and density of the Tourte are 27.8 GPa and 1.12 g/cm^3 with μ equal to 22.1.

Estimates for the modulus and density of the Peccatte are 27.2 GPa and 1.07 g/cm^3 with μ equal to 23.9. A difficult and poor estimate of graduations under the grip probably accounts for the odd variation near the frog. My four most recent bows are based on a linearized stiffness model of this Peccatte shown above, and plotted in Fig. 13 with

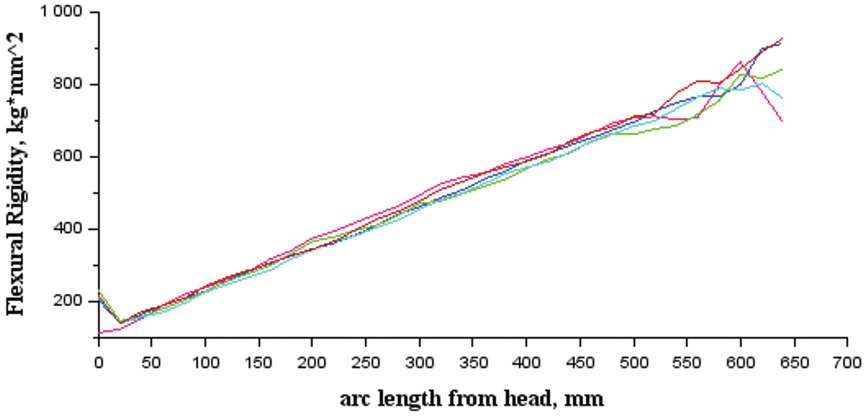

Figure 13. Local stiffness of Peccatte in red, together with four bows of similar design.

the Peccatte in red and the others with values of μ equal to 22.1, 24.5, 25.7, and 26.5 in GPa.

With E and μ in GPa, consider the bow blanks A and B selected from those in Figs. 1 and 2 with the following properties:

Table 1. E and μ in GPa, ρ as specific gravity and c in m/s.

	E	ρ	μ	c
A	22.8	0.96	25.04	4890
B	31.3	1.12	25.01	5288

Although A is a floater, with both modulus and density considerably smaller than B, their values of μ are virtually identical. Round tapers shown in Fig. 14 and listed in Table 2 were designed for both A and B such that each reproduces the linearized local stiffness model of the Peccatte.

The decrease in diameter in approaching the forward frog position is a result of the gradual linear conversion from round to octagonal for the frog section. The increasing cross-sectional moment of inertia over a round section allows their diameter to gradually decrease, while still maintaining linearly increasing stiffness. For a regular octagonal bow, the diameter continues to increase to produce linear stiffness to the frog. From the comparison between round and octagonal cross sections in Section 5, an octagonal bow, with the same local stiffness function as a round alternative, will be about 5.3% lighter between the head and frog.

The head and frog heights were carefully chosen so that their effective moment arms relative to the neutral axis were very close in value and the resulting bows are assumed fully cambered. Using the geometry defined by these graduations, notwithstanding their different densities and tapers, the computed mass of the sections between the head and frog in Eqn. (12) are nearly identical,

$$w'_{\mathrm{A}} = 30.49 \quad w'_{\mathrm{B}} = 30.51, \tag{53}$$

demonstrating that blanks with the same value of μ can reproduce both mass and local stiffness between the head and frog of a desired target with proper taper design. The floater A is the equal of the more typically prized higher density B. The differences in the cantilever mode frequencies can then be reduced or possibly eliminated by careful tuning of the head shapes, with that of higher density B likely smaller than A. The remaining total weight and balance issues then depend on the selections of grip, frog, and button.

10. DAMPING RATIO

Any player knows that in going through a box of bows, some will be louder than others and also produce different harmonic content from the same instrument. Although the vibrating mode

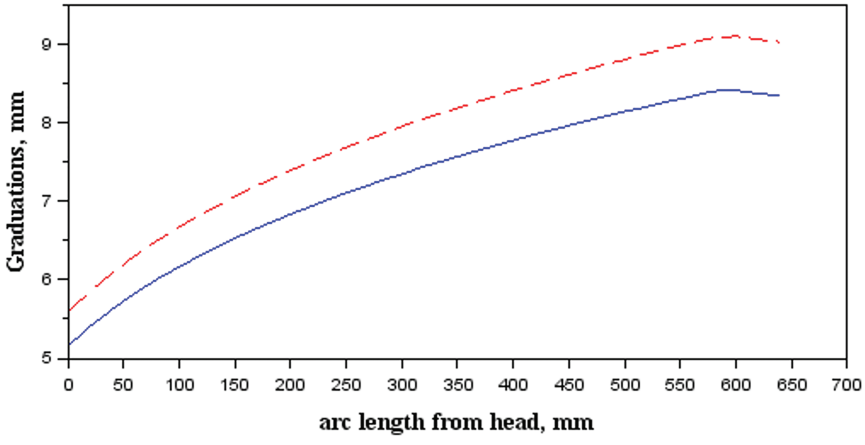

Figure 14. Round graduations for blanks A and B as functions of arc length between the head and forward frog position. A dashed, B solid.

Table 2. Round graduations in mm for blanks A and B, together with their local stiffness and that of the linearized Peccatte model.

	Floater		Sinker		Linearized Peccatte
s	D_A	$E_A I_A$	D_B	$E_B I_B$	Stiffness Model
0	5.59	111.29	5.16	111.29	111.07
20	5.86	134.41	5.41	134.41	134.15
40	6.09	157.53	5.63	157.53	157.22
60	6.31	180.64	5.83	180.65	180.29
80	6.50	203.76	6.01	203.76	203.36
100	6.68	226.87	6.17	226.88	226.43
120	6.84	249.99	6.32	250.00	249.50
140	6.99	273.11	6.46	273.11	272.58
160	7.14	296.22	6.60	296.23	295.65
180	7.27	319.34	6.72	319.35	318.72
200	7.40	342.46	6.84	342.47	341.79
220	7.52	365.57	6.95	365.58	364.86
240	7.64	388.69	7.06	388.70	387.93
260	7.75	411.81	7.16	411.82	411.00
280	7.85	434.92	7.26	434.93	434.08
300	7.96	458.04	7.35	458.05	457.15
320	8.06	481.16	7.45	481.17	480.22
340	8.15	504.27	7.53	504.28	503.29
360	8.24	527.39	7.62	527.40	526.36
380	8.33	550.51	7.70	550.52	549.43
400	8.42	573.62	7.78	573.64	572.50
420	8.50	596.74	7.86	596.75	595.58
440	8.58	619.86	7.93	619.87	618.65
460	8.66	642.97	8.01	642.99	641.72
480	8.74	666.09	8.08	666.10	664.79
500	8.81	689.21	8.15	689.22	687.86
520	8.89	712.32	8.21	712.34	710.93
540	8.96	735.44	8.28	735.46	734.00
560	9.03	758.56	8.34	758.57	757.08
580	9.09	781.67	8.41	781.69	780.15
600	9.11	804.79	8.42	804.81	803.22
620	9.07	827.90	8.38	827.92	826.29
639	9.04	849.87	8.35	849.88	848.21

frequencies of the bow are of course involved, the inherent damping of the wood in the bow is also an important factor in the outcome.

The same cantilever setup used to measure the modulus of elasticity [7] in Section 6 was also used to estimate the damping ratio by exciting free vibration in the vertical plane and sampling the exponentially decaying sinusoidal signal in Fig. 15 at 8 kHz for 4 s. While this can be difficult in a finished bow because of very close vertical and horizontal fundamental mode frequencies, a blank, especially if rectangular, is usually more successful. Nevertheless, for a finished bow clamped at the forward frog position, analysis of the data can estimate the fundamental mode frequency useful in the subsequent head design.

For damped, free vibration, the response can often be approximated by an exponentially decaying sinusoid [13] of the form

$$v = X_0 e^{-\zeta\omega_n t} \sin\left(\omega_n \sqrt{1-\zeta^2}\, t + \varphi\right) + X_1 \quad (54)$$

with natural angular frequency ω_n and damping ratio ζ. Although ζ can be approximated by the method of logarithmic decrement [13], here we need estimates of both ζ and the damped natural angular frequency ω_d given by

$$\omega_d = \omega_n \sqrt{1-\zeta^2}. \quad (55)$$

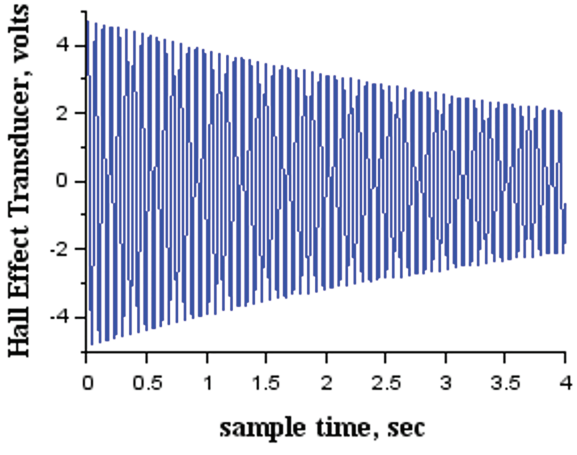

Figure 15. Exponentially decaying response of unfinished octagonal violin bow with damping ratio 0.0021 and fundamental frequency 15.46 Hz.

After approximating ζ using logarithmic decrement as an initial value in the optimization, the model in Eqn. (54) or a sum of two such models is fitted in a least squares sense for the decay constant $\zeta\omega_n$, ω_d and the other parameters, then yielding the damping ratio ζ and the fundamental mode frequency $f_d = 2\pi\omega_d$. Because of its complexity, particularly when a sum of two models is used in the case of two vibrating modes, this fitting was done using the genetic optimization method known as Differential Evolution [14].

For the same set of 50 violin bow blanks in Section 4, Fig. 16 is a plot of the damping ratio as a function of μ where the range of the modulus E is mapped to the light-to-dark color map with light the smallest values of E and dark the largest. The linear least squares fit reveals a trend of decreasing damping with increasing μ but with the lowest damping usually found in higher values of E.

11. ITERATIVE DESIGN PROCEDURE

For a given target bow without hair, measuring its graduations and using the appropriate cross-sectional model in Section 5 produces a geometrical model of the bow. Unfortunately, most desirable targets have a grip winding and leather wrap and their mass and centers of mass need to be estimated together with a model of the head to obtain a rough estimate of the density ρ from the total mass and balance of the stick. This is of course especially important in the case of a metal tip. An accurate model of the frog section is also required.

At points 20 mm apart along the bow, the measured graduations then are used to compute the vertical cross-sectional moment of inertia I_x at each point, either directly from Eqn. (19) for an octagonal bow or Eqn. (24) for a round bow after generating a periodic spline model of the cross-sectional shape $D(\lambda)$. These cross-sectional models at points along the bending section of the bow can then be used to compute weight and moment from Eqns. (4) and (5) together with the location of the center of mass of section between head and frog in Eqn. (7). After adding models of the head and frog section volumes and centers of mass, measurements of the total

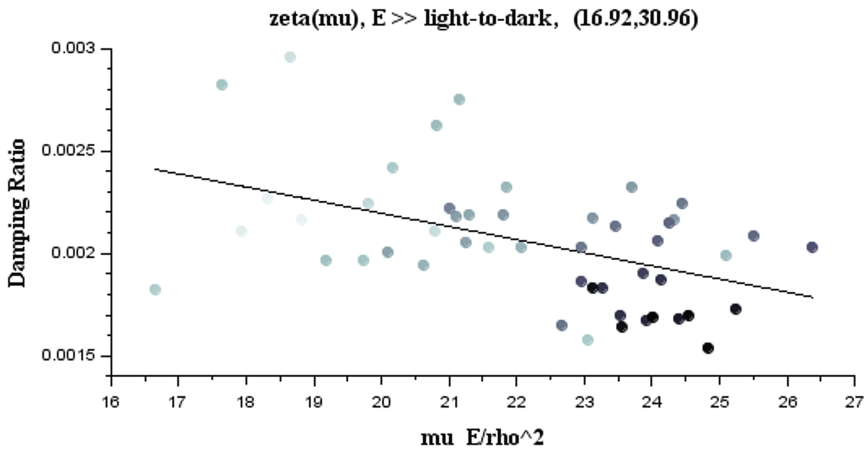

Figure 16. Variation of damping ratio with μ and including light-to-dark point shade mapped to increasing values of the modulus of elasticity, E on the interval (16.92, 30.96) in GPa.

stick mass and center of mass then provide two equations solved for the density and volume of the head. We now have a geometric model of the bow and its density estimate ρ_t.

Using the cantilever setup in Section 6, the target is carefully clamped at its forward frog position and the static deflection test is performed obtaining the deflection δ under the load F just behind the head. This setup using the method in Section 10 can also find the fundamental mode frequency and perhaps the damping ratio as well. Solving the corresponding tapered curved beam boundary problem results in an estimate for the average modulus E_t of the target bow, and in turn produces an estimate of the target bow value of $\mu_t = \frac{E_t}{\rho_t^2}$. Estimating μ for a bow blank is a considerably simpler process, given the typically rectangular shape of both the cross section and the head.

Selecting a blank with a similar value of μ as the target then provides the blank values of E_b and ρ_b. Unless attempting to reproduce the scaled target cross-sectional shape at every point along the stick, the alternative round taper in Eqn. (32) or regular octagonal taper in Eqn. (33) should be used as the target taper in Eqn. (2) and the resulting blank taper D_b is obtained.

After roughing out an initial oversized vertical taper D_b in the stick, the wood is evaluated again in its true rectangular cross-sectional shape, generating new estimates for E and ρ. This is an especially good time to measure the damping ratio as mentioned in Section 10. The wood evaluation is repeated in the approximate square and then octagonal cross-sectional states, each time generating a new target taper D_b for the blank by the same process. Whether remaining octagonal or continuing on to a round cross section, the iterations continue and gradually remove less and less wood as the final target is approached. When satisfied with the final graduations between the head and frog, the method in Section 10 is used to estimate the fundamental cantilever mode frequency, f_d. Adjusting the mass of the head can then be done, gradually bringing this frequency closer to the target to adjust for differences in density.

This entire iterative process is easier to perform before the stick is cambered. If necessary, the camber profile for the bow can then be calculated from Eqns. (49) and (50), producing the camber that will be simply undone when tightening the hair. The remaining frog, button, and grip selection completes the process.

Given the interesting linear stiffness property of the Tourte model described in Section 9, a linearized stiffness model of the Peccatte in Fig. 12 was generated and used as the target design for the bows shown in Fig. 13 along with the Peccatte in red. These four bows with different

values of μ were only designed to reproduce the linear stiffness of the Peccatte model, with the final outcome determined by tip geometry, grip, frog, and button selections. The consistent and remarkably linear stiffness outcomes of these bows is the result of this iterative process.

12. CONCLUSIONS

A process for reverse engineering bows has been outlined, with wood selection using the parameter $\mu = \frac{E}{\rho^2}$, and new taper computed from the target, guaranteeing that both the mechanical bending, mass, and moment properties between the head and forward frog position are reproduced exactly. Furthermore, the cantilever vibrating mode frequencies can also be reproduced by adjusting the head mass. While wood selection based on the speed of sound measurement has been helpful, it inflates the value of very high-density wood while penalizing many floaters that can be turned into high-quality bows. The value of the parameter μ serves as a direct measure of the stiffness and mass properties of the bending section of the bow and clearly represents the expected possible outcome from a given piece of wood.

Future Work

Obtaining accurate estimates of the modulus and density can be improved by making better use of the available data. While the mass and center of mass measurements are only a function of density and geometry and the deflection under load is only affected by the modulus and geometry, the fundamental mode frequency of vibration in the cantilever experiment is a function of all three, resulting in four equations for the two unknowns E and μ. The velocity of sound condition in Eqn. (15) could also be added. In either case, this leads to an overdetermined system of equations that could be attacked with weighted nonlinear least squares that incorporates likely experimental measurement error.

NOMENCLATURE

E,	modulus of elasticity in GPa
ρ, rho	mass density in grams per cm^3 or its numerical equivalent of dimensionless specific gravity
μ, mu	wood selection parameter in GPa
c,	speed of sound in m/s
L_s,	arc length of bow between head and forward frog position in mm
D,	diameter of perfectly round or regular octagonal cross section in mm
w',	weight of the stick between the head and forward frog position in grams
m',	first moment of weight of the stick between the head and forward frog position, with respect to that position in gram mm
i',	second moment of weight of the stick between the head and forward frog position, with respect to that position in gram mm^2.
x_m,	horizontal moment arm of cross-sectional area with respect to the forward frog position in mm
cm,	horizontal distance of center of mass of bending section from forward frog position in mm
w,	width of rectangular cross section in mm
h,	thickness of rectangular cross section in mm
V,	vertical thickness of octagonal or spline cross section in mm
U,	upper thickness of octagonal or spline cross section in mm
H,	horizontal thickness of octagonal or spline cross section in mm
L,	lower thickness of octagonal or spline cross section in mm
λ,	angle clockwise positive from vertical for oval spline model in radians
A,	cross-sectional area in mm^2
I_x, I	vertical cross-sectional moment of inertia in mm^4
I_y, J	horizontal cross-sectional moment of inertia in mm^4
σ,	arc length along the bow measured from the forward frog position in mm
$\varnothing(\sigma)$,	tangent angle as function of arc length under cantilever load F in radians
$\varnothing_0(\sigma)$,	tangent angle as function of arc length of initial camber in radians
F,	cantilever load in kg
M,	distance of load from cantilever support in mm
y,	y coordinate of neutral axis under cantilever load in mm

y_0, y coordinate of neutral axis of initial camber in mm
δ, vertical deflection of beam at the cantilever load in mm
U, elastic strain energy under load
Ω, potential energy of the external load
Π, total potential energy
D_R, round taper with equivalent I_x to target design in mm
s, arc length along the bow measured from just behind the head in mm
a, perpendicular distance from neutral axis at head to line of action of the hair in mm
b, perpendicular distance from neutral axis at frog to line of action of the hair in mm
$\theta(s)$, tangent angle as function of arc length under hair tension T in radians
$\theta_0(s)$, tangent angle as function of arc length of initial camber in radians
L_T, arc length coordinate of frog under hair tension in mm
L_0, arc length coordinate of horizontal tangent to neutral axis in mm
T, hair tension in kg
$\overline{T}$, maximum hair tension producing a linear neutral axis in kg
L_S, arc length coordinate of frog at maximum hair tension $\overline{T}$ with linear neutral axis
β, constant tangent angle at maximum hair tension $\overline{T}$
l_0, horizontal distance along hair with zero tension in mm
l, horizontal distance along hair under tension T in mm
$x_0(s)$, x coordinate of neutral axis at initial camber in mm
$y_0(s)$, y coordinate of neutral axis at initial camber in mm
$V(L_0)$, vertical thickness of stick at L_0 in mm
ε, distance between bottom of the stick and table with finished frog and head in mm
X_0, damping model amplitude
X_1, damping model offset
ϕ, damping model phase
ζ, zeta dimensionless damping ratio
ω_n, undamped natural angular frequency in rad/s
ω_d, damped natural angular frequency in rad/s
f_d, fundamental mode frequency in Hz

REFERENCES

[1] E.S. Alves, E.L. Longui, and E. Amano, Pernambuco wood (*Caesalpinia echinata*) used in the manufacture of bows for string instruments, *IAWA J.,* Vol. 29, No. 3, pp. 323–35 (2008).

[2] U.G.K. Wegst, Wood for sound, *Am. J. Bot.,* Vol. 93, No. 10, pp. 1439–48 (2006).

[3] Panel Discussion, Innovation in bowmaking, *J. Violin Soc. Am. Proc.,* Vol. XXIII, No. 3, pp. 1–8 (2012).

[4] R.J. Ross, *Nondestructive Evaluation of Wood* (2nd ed. U.S. Department of Agriculture, Washington, DC, 2015).

[5] K. Guettler, *Some Physical Properties of the Modern Violin Bow* (Norwegian Academy of Music, Oslo, Norway, 2006).

[6] A.C. Ugural and S.K. Fenster, *Advanced Mechanics of Materials and Applied Elasticity* (6th ed. Pearson, London, 2019).

[7] M. Ciornei, E. Diaconescu, and M. Glovnea, Experimental investigations of wood damping and elastic modulus, DOCT-US, an I, nr. 1, 2009.

[8] S.S. Rao, *Vibration of Continuous Systems* (John Wiley & Sons, Hoboken, NJ, 2007).

[9] C.L. Dym and I.H. Shames, *Solid Mechanics, A Variational Approach* (Augmented ed. Springer, New York, NY, 2013).

[10] J.M. Ortega and W.G. Poole, Jr., *An Introduction to Numerical Methods for Differential Equations* (Pittman Publishing Inc, London, 1981).

[11] C. Gough, The violin bow: Taper, camber and flexibility, *J. Acoust. Soc. Am.,* Vol. 130, No. 6, pp. 4105–16 (Dec. 2011).

[12] F. Ablitzer, J.-P. Dalmont, and N. Dauchez, Static model of a violin bow:

Influence of camber and hair tension on mechanical behavior, *J. Acoust. Soc. Am.,* Vol. 131, No. 1, Pt. 2 (Jan. 2012).

[13] M.L. James, G.M. Smith, J.C. Wolford, and P.W. Whaley, *Vibration of Mechanical and Structural Systems with Microcomputer Applications* (Second Edition, Harper Collins College Publishers, 10 East 53rd Street, New York, NY 10022, 1994).

[14] R. Storn and K. Price, Differential evolution—A simple and efficient heuristic for global optimization over continuous spaces, *J. Glob. Optim.,* Vol. 11, No. 4, pp. 341–59 (1997).